Seismic Upgrading Performance of Steel Frames Installed with SMA Dampers

Xiao-Qun Luo[1], Hanbin Ge[2] and Tsutomu Usami[3]

[1]Doctor, Post Doctoral Researcher, ARCSEC, Meijo University (1-501 Shiogamaguchi, Tempaku-ku, Nagoya, 468-8502)
[2]Member, Dr.Eng., Professor, Dept. of Civil Engineering, Meijo University (1-501 Shiogamaguchi, Tempaku-ku, Nagoya, 468-8502)
[3]Fellow, Dr.Sc., Professor, Dept. of Civil Engineering, Meijo University (1-501 Shiogamaguchi, Tempaku-ku, Nagoya, 468-8502)

1. Introduction

Damping devices are usually applied for suppression of undesired structural vibrations under severe loadings such as strong earthquake motions. With development of new materials and new control techniques, many damping devices are developed such as viscous dampers, visco-elastic dampers, friction dampers, hysteretic metal dampers, shape memory dampers and so on.

Shape memory alloys (SMAs) are smart metallic materials that can undergo large deformations over 10% and return to their original shape without residual deformations through heat process or removal of load. These unique properties led to applications in biomedical field, aerospace field and commercial industry. Recently, due to the fairly intelligent characteristics of SMAs such as re-centering, energy dissipating, damping and so on, SMAs are also used in seismic design for civil engineering and building engineering [1]. Experiments, numerical models and applications on SMA dampers were present by many researchers but most of them were still in laboratory stage [2].

Here, a kind of SMA damper developed for seismic upgrading is introduced, its numerical model is presented based on a simple multi-linear one dimensional constitutive law of SMAs and the effectiveness is verified under detailed dynamic analysis and comparisons.

2. Constitutive Models of SMAs

In order to simulate the material behavior of SMAs numerically, microscopic methodology and macroscopic methodology are two approaches which focus on molecular level and phenomenological features of SMAs, respectively [3), 4)]. A simple multi-linear one dimensional constitutive model based on the thermodynamic laws is formulated with different metallographic phase fractions.

The special expression of Gibbs free energy can be derived from the possible single-phase material form recommended by Reniecki, shown as equation (1):

$$\begin{aligned} G(\varepsilon,\xi,T) = {} & [(u_A - Ts_A) - \xi(\Delta u - T\Delta s)] \\ & + C\left[(T-T_0) - T\ln\frac{T}{T_0}\right] + \frac{1}{2}E[\varepsilon-\varepsilon_L]^2 \\ & - (T-T_0)[\varepsilon-\varepsilon_L\xi]Ec \end{aligned} \tag{1}$$

where u_A and s_A are the internal energy and the entropy of the austenite; ξ is the fraction of the martensite; Δu and Δs are difference of the internal energy and the entropy between the austenite and martensite; C, T_0, E, ε_L, c are heat capacity, reference temperature, elastic modulus, residual strain and thermal expansion factor, respectively.

Considering the standard relationship among free energy, stress and strain, from equation (1), we get:

$$\sigma = \frac{\partial G}{\partial \varepsilon} = E[\varepsilon - \alpha(T-T_0) - \varepsilon_L\xi] \tag{2}$$

In transformation processes, the module of E is the function of elastic modules in austenite and martensite types and is related to their fractions. We can get the module of E simply as follows:

$$E = \frac{E_A E_M}{\xi E_A + (1-\xi)E_M} \tag{3}$$

For constructing multi-linear constitutive model, a linear stress-strain relationship is assumed between every two transformation stresses:

$$\sigma = a\varepsilon + b \tag{4}$$

Then varied martensite fraction ξ in the forward transformation process and the reversal transformation process can be derived in explicit formulation from equations (2)-(4):

$$\xi = \frac{E_A E_M [\varepsilon - \alpha(T - T_0)]}{(a\varepsilon + b)(E_A - E_M) - E_A E_M \varepsilon_L} \tag{5}$$

The proposed constitutive model can be easily illustrated in Fig.1. As shown in Fig.1(a), for SMA in the austenite state, if transformation stresses σ_{MS}, σ_{MF}, σ_{AS} and σ_{AF} are known, the bone curve of the multi-linear constitutive model is easily plotted. Shown in Fig.1(b) is the detwinning process of SMA in the martensite state, where the start and finish critical stresses are named σ_{MSCR}, σ_{MFCR}, and the initial stiffness and stiffness after detwinning are all E_M.

If unloading occurs before completion of forward transformation or reloading occurs before completion of reversal transformation, the subloop paths are introduced also in Fig.1(a). The elastic module in the unloading and reloading phase is equal to the module at the unloading or reloading point with martensite fraction ξ and the transformation stresses in subloop paths are on the diagonal line between σ_{MS} and σ_{AS}.

3. Numerical Model of Axial-type SMA Damper

An axial-type SMA damper is shown in Fig.2(a) that two blocks (i.e., Part A and Part B) made of steel can slide past each other and two sets of austenite wire systems and one martensite bar are kernel materials in the damper that the martensite bar can afford tension and compression without undergoing buckling and two sets of austenite wire are tension only and react in reverse directions. The corresponding analytical model of the damper is shown in Fig.2(b) that combined by three separate schematic plots acted as austenite wires in positive direction, austenite wires in reverse direction and martensite bar, respectively.

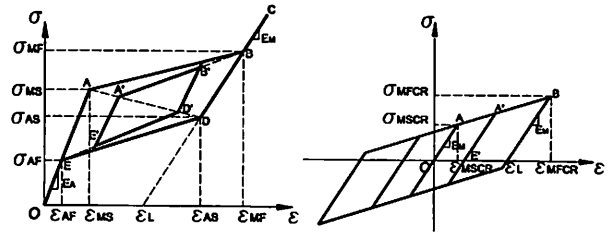

(a) General model (b) Model of martensite detwining

Fig.1 Constitutive models for SMA

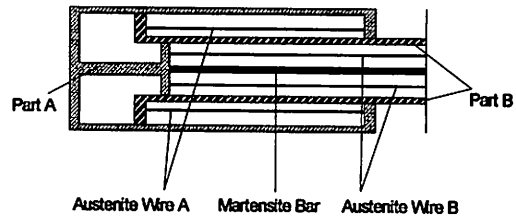

(a) SMA damper prototype

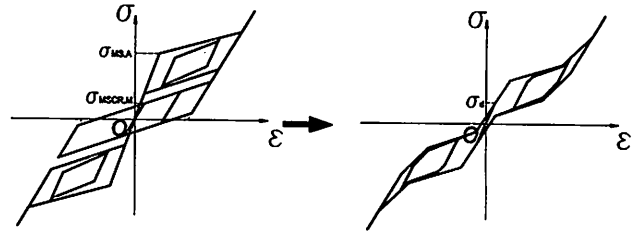

(b) Constitutive law of the damper

Fig.2 Prototype and stress-strain relationship of SMA damper

4. Design and modeling of SMA damping devices

As in a previous study of controlled structures[5], three parameters, i.e. the strength ratio α_F, the stiffness ratio α_K and the displacement ratio α_δ, are proposed as design criteria shown below:

$$\alpha_F = \frac{F_{y,d}}{F_{y,f}} \quad \alpha_k = \frac{K_{y,d}}{K_{y,f}} \quad \alpha_\delta = \frac{\delta_{y,d}}{\delta_{y,f}} \tag{6}$$

here, $F_{y,d}$, $K_{y,d}$ and $\delta_{y,d}$ are elastic stiffness, yield displacement and yield strength of damping devices, respectively, while $F_{y,f}$, $K_{y,f}$ and $\delta_{y,f}$ are those of main structures.

Geometric parameters and basic properties of a SMA damping devices are illustrated in Fig.3. $(EA)_{SMA}$, l_{SMA} and $(EA)_{SMA}$, l_b are stiffness and length of SMA and steel bar, respectively. F_{SMA}, K_{SMA} and δ_{SMA} are lateral yield force, elastic stiffness and displacement of a pair of SMA-combined dampers,respectively. Assuming α_L and β_L as two scales on length and stiffness between SMA

component and steel component, relationship between these parameters can be expressed as follows:

$$F_{SMA} = K_{SMA}\delta_{SMA} \tag{7}$$

$$l = l_{SMA} + l_b, \quad l_b = \alpha_L l_{SMA}, \quad (EA)_b = \beta_L (EA)_{SMA} \tag{8}$$

$$C_1 = \frac{2}{(1+\alpha_L)}\left(1+\frac{\alpha_L}{\beta_L}\right) \tag{9}$$

$$K_{SMA} = A_{SMA} \cdot \frac{1}{C_1}\frac{E_{SMA}L^2}{l^3} \tag{10}$$

$$\delta_{SMA} = \frac{\sigma_{SMA}}{E_{SMA}}\frac{l^2}{L}C_1 \tag{11}$$

$$F_{SMA} = \sigma_{SMA} A_{SMA}\frac{L}{l} \tag{12}$$

Here, α_L=0 means that the damper is designed by full SMA component and β_L=∞ means that the stiffness of the steel bar is assumed to be rigid.

5. Examples and Results

A benchmark frame FA is a 12×12m square-shaped plane frame, which is shown in Fig. 4, bare main frame in (a), frame with damper in (b), and sections of girders and piers are shown in (c). The benchmark frame is made of SM490 steel grade and details of the frame can be found in previous studies[6]. The SMA material constants are given in Table 1. The yield shear force and top displacement of the bare main frame given in Table 2 is determined with a pushover analysis.

Four strong ground motions are considered in analyses, three of which are recommended in the JRA code[7], JRT-EW-M, JRT-NS-M and FUKIAI-M and the other is LA16 designed by SAC[8].

In order to invstigate the seismic upgrading performance of frames with SMA dampers, performace parameters to be investigated include as follows:

1) maximum top displacement, δ_{max} ;
2) maximum base shear, V_{max};
3) residual top displacement, δ_{res};
4) normalized axial strain of dampers, $\varepsilon_{max}/\varepsilon_y)_{SMA}$; and
5) average compressive strain in piers, $\varepsilon_{a),max}$.

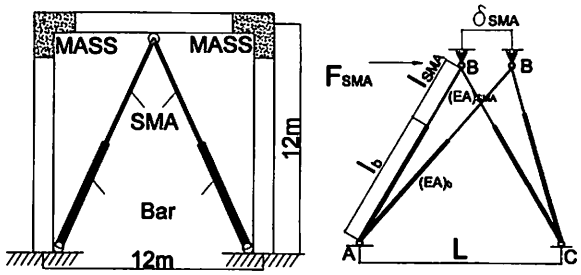

(a) Frame (b) Schematic diagram for SMA deformation

Fig.3 Models of frame and SMA damper

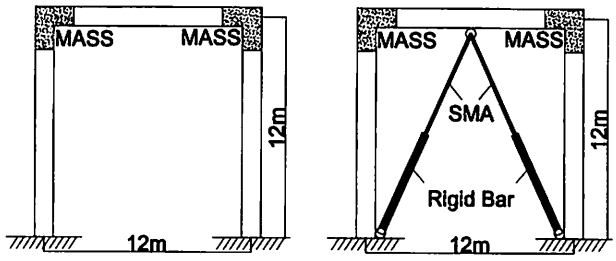

(a) Bare frame (b)frame with dampers

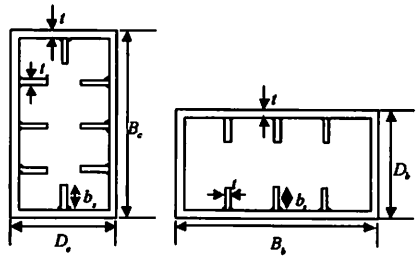

(c) Sections of frame girders and piers

Fig.4 Benchmark frame type

Table1 SMA material constants

E_A(Gpa)	E_M(Gpa)	ε_L	T(℃)
70	30	0.05	40
σ_{MS}(Mpa)	σ_{MF}(Mpa)	σ_{AS}(Mpa)	σ_{AF}(Mpa)
235	325	210	100
σ_{MSCR}(Mpa)	σ_{MFCR}(Mpa)		
100	170		

Table2 Basic information of the bare frame

Name	M(Kg)	V_y (KN)	$\delta_{y,top}$ (m)
FA	2042	6758	0.078

Here the five performance parameters are evaluated under considerations of four influence factors listed as follows:

1) strength ratio, α_F;
2) martensite fraction of SMA dampers, ξ;
3) length ratio, α_L; and
4) ground motions.

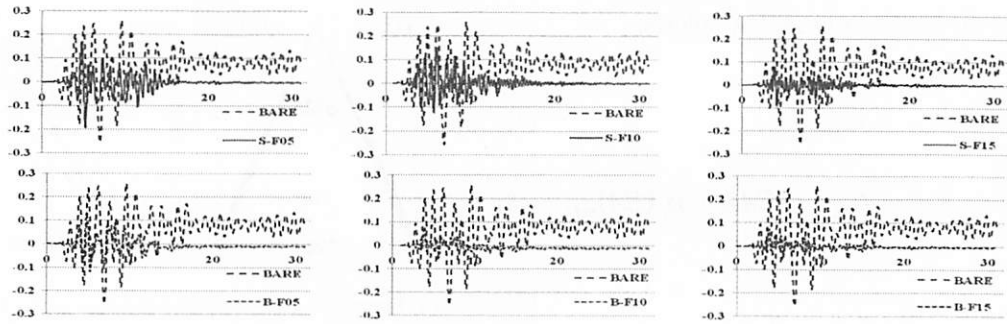

(a) Top displacement response

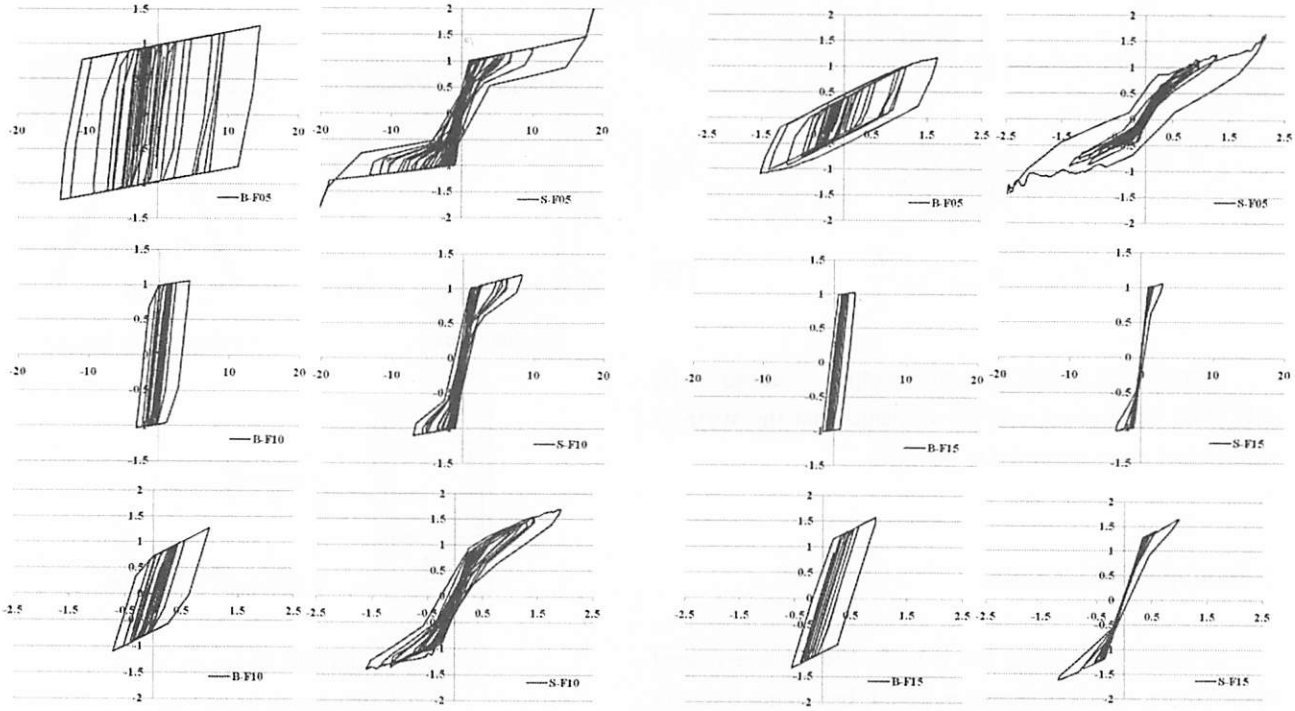

(b) Stress-strain response of dampers

(c) Base shear-top displacement responses

Fig. 5 Comparisons between the BRB models and SMA models with different strength ratios

(1) Effects of strength ratio α_F

Only JRT-EW-M accelerogram is used for time-history analysis in this subsection. Equivalent frames with BRB dampers are designed with the same strength ratio α_F and stiffness ratio α_K as frames with SMA dampers for comparison, and the basic information of SMA models and BRB models are shown in Table 3. The response results are illustrated in Fig.5 and maximum seismic responses are listed in Table 4.

Shown in Fig.5(a) are the time history responses of top displacement for SMA model and BRB model together with the bare frame. Compared to the bare frame, it can be seen that the displacement demands are greatly reduced in both the SMA models and BRB models. With the same strength ratio, comparisons bewteen the BRB models and SMA models indicate that the maximum top displacement in the SMA models is a little larger, but the residual top displacement is less than those in the BRB models. Shown in Fig.5(b) are the stress-strain responses of dampers, with the same α_F, the hysteretic loops in SMAs are a little shallower than in BRBs. Relationships between the total base shear and top displacement of damped frames are shown in Fig.5 (c), and the maximum base shear and maximum top displacement in the SMA models are larger than those in the BRB models.

Table 4 represents normalized maximum responses obtained from time-history analysis. Compared to the bare frame, significant reductions can be seen in all the performance parameters except for the maximum base shear, which means the substantial seismic upgrading obtained by setting damping devices. From comparisons between the BRB models and the SMA models, with the same α_F and α_K, it is found that the efficiency of the BRB models is better than the SMA models except for the

ability of re-centering. E.g., in the case of α_F=1.0, the residual top displacement in the SMA models reaches to $0.002\delta_y$ while $0.151\delta_y$ in the BRB models, and the maximum average strain at the base of piers in the BRB models are nearly $0.9\varepsilon_y$, while $1.4\varepsilon_y$ in the SMA models which is still less than $2.0\varepsilon_y$, which is required for the performance level 2[9].

The facts revealed in Fig.5 and Table 4 suggest that the seismic demands of frames with SMA dampers can be effectively controlled in light damage, although the energy dissipating ability of the BRB dampers is better than the SMA's. However, the recentering ability in the SMA models is far better than those in the BRB models so that it is useful for reducing permanent deformation in structures under strong earthquakes.

(2) Effects of martensite fraction ξ in SMA dampers

Only JRT-EW-M accelerogram, the strength ratio α_F=1.0 and the length ratio α_L=4.69 are used here. Five different martensite fractions, i.e., 0%, 25%, 50%, 75% and 100%, are considered. Because of different start transformation stresses in austenite and martensite types, area of SMA are calculated based on equation (12).

Fig.6 shows time history response of base shear versus top displacement under differenet martensite fractions from 25% to 100%, and the case of pure autenite SMA is the same as S-F10 in Fig.5(c). As the content of martensite SMA increases, the maximum base shear decreases from nearly $1.7V_y$ in pure austenite SMA to below $1.4V_y$, and the same trendency can be observed in the maximum top displacement. The normalized maximum responses from time history analyzes are shown in Table 5. As we can see, investigated performaces of δ_{max} , V_{max} and $\varepsilon_{a)max}$ are improved with inceasing content of martensite SMA, but the performance of δ_{res} decreases because of lack of super elasticity in martensite SMAs.

(3) Effects of length ratio α_L in damper systems

Only JRT-EW-M accelerogram, the strength ratio α_F=1.0 and the martensite fraction ratio ξ=0 are used here. Five different length ratio, i.e., 1, 2, 4, 6 and 4.69, are considered. The case of 4.69 is the same as the cases S-F10 and M00 in the subsections (1) and (2).

Under the conditions of the same SMA area and martensite fractions, the bigger the length ratio, the larger the stiffness of the damped brace system. From the normalized maximum responses shown in Table 6, with

Table3 Basic information of BRB and SMA models

Name	α_F	α_K	σ_y(Mpa)	A (m^2)	α_L
BF05	0.5	6.318	59.3	0.092	--
BF10	1.0	6.414	118	0.093	--
BF15	1.5	6.419	172	0.093	--
SF05	0.5	6.318	235	0.023	10.3
SF10	1.0	6.414	235	0.047	4.69
SF15	1.5	6.419	235	0.068	2.90

Note: BF and SF represent BRB models and SMA models, and xx means the values of the strength ratio α_F.

Table4 Maximum responses under effects of α_F

No	Time history analysis results				
	$\frac{\varepsilon_{a)\max}}{\varepsilon_y}$	$\frac{\delta_{\max}}{\delta_{y,f}}$	$\frac{\delta_{res}}{\delta_{y,f}}$	$\frac{V_{b,\max}}{F_{y,f}}$	$\left(\frac{\varepsilon_{\max}}{\varepsilon_y}\right)_{SMA}$
Bare	20.409	3.333	0.981	1.192	--
BF05	2.009	1.687	0.138	1.095	14.521
SF05	3.765	2.152	0.0233	1.645	18.844
BF10	0.889	0.995	0.151	1.275	4.356
SF10	1.433	1.914	0.0020	1.698	8.379
BF15	0.653	0.945	0.0459	1.573	2.835
SF15	0.731	1.001	0.0080	1.648	3.055

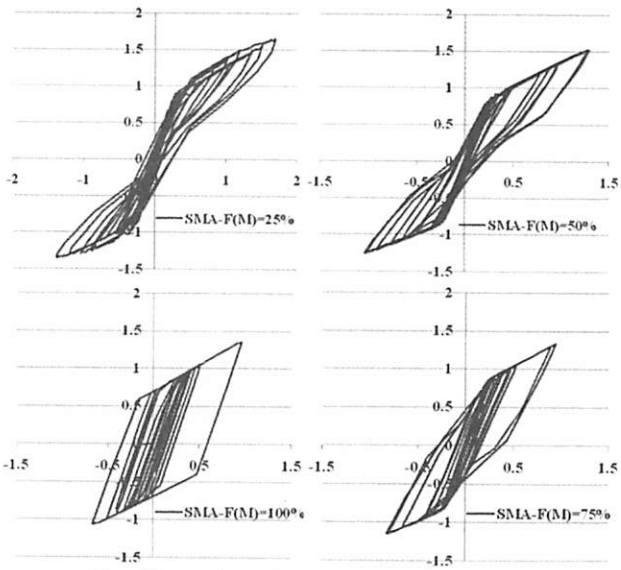

Fig. 6 Base shear-top displacement responses with different martensite fraction ratios ξ

Table5 Maximum response under effects of ξ

No	Time history analysis results				
	$\frac{\varepsilon_{a)\max}}{\varepsilon_y}$	$\frac{\delta_{\max}}{\delta_{y,f}}$	$\frac{\delta_{res}}{\delta_{y,f}}$	$\frac{V_{b,\max}}{F_{y,f}}$	$\left(\frac{\varepsilon_{\max}}{\varepsilon_y}\right)_{SMA}$
M00	1.433	1.914	0.0019	1.698	8.379
M25	1.404	1.684	0.008	1.640	7.476
M50	1.346	1.289	0.028	1.516	5.773
M75	0.856	0.932	0.040	1.428	4.262
M100	0.706	0.829	0.034	1.396	4.105

the length ratio increasing, all investigated performaces of δ_{max} , V_{max}, $\varepsilon_{a)max}$ and δ_{res} are improved, and $\varepsilon_{max}/\varepsilon_{y)SMA}$ increases rapidly mainly because the length of SMA damper is shorten with the increased length ratio.

(4) Effects of various Level-II ground motions

To further investigate efficiency of dampers under various ground motions, except for aforementioned JRT-EW-M, three other ground motions JRT-NS-M, FUKIAI-M and LA16 are employed, and the bare frame, equivelent frames with BRB and SMA under α_F=0.5 are adopted, respectively.

The result comparisons are illustrated in Fig. 7. Compared to the bare frame, it is clear as mentioned previously that each performance demand in the damped frames has a large reduction except for the base shear force. Comparing between the BRB models and SMA models, it is seen that most performance indics of the SMA models are larger than the BRB models, particularly in JRT-NS-M and FUKIAI-M cases. The residual top displacements of SMA models are far less than those of BRB models in JRT-EW-M and LA16 cases but almost equal in JRT-NS-M and FUKIAI-M cases. It is shown that the SMA model is much more sensitive to earthquake inputs.

6. Conclusions

An axial-type SMA damper is proposed and its numerical model is present here based on a multi-linear one dimensional constitutive SMA model. Time history analyzes are carried out on a benchmark frame in consideration of different performance parameters and different damping devices to evaluate the seismic upgrading performance of steel structures with the SMA damper. The results demonstrate that SMA is effective on seismic upgrading especially re-centering performance, and SMA is sensitive to earthquake inputs.

Acknowledgement: The study was supported in part by grants from the Advanced Research Center for Seismic Experiments and Computations, Meijo University.

Table6 Maximum responses under effects of α_L

No	Time history analysis results				
	$\frac{\varepsilon_{a)\max}}{\varepsilon_y}$	$\frac{\delta_{\max}}{\delta_{y,f}}$	$\frac{\delta_{res}}{\delta_{y,f}}$	$\frac{V_{b,\max}}{F_{y,f}}$	$\left(\frac{\varepsilon_{\max}}{\varepsilon_y}\right)_{SMA}$
L4.69	1.433	1.914	0.0019	1.698	8.379
L1	1.917	2.047	0.0695	1.574	3.060
L2	1.831	1.904	0.0491	1.569	4.343
L4	1.512	1.927	0.0134	1.685	7.393
L6	1.585	1.858	0.0131	1.735	10.192

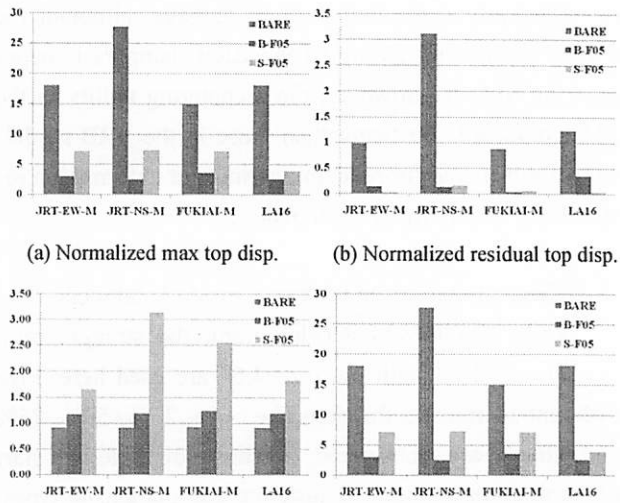

(a) Normalized max top disp. (b) Normalized residual top disp.

(c) Normalized max shear force (d) Normalized average strain at piers

Fig. 7 Comparison under various strong earthquakes

References

1) K. Wilde, P. Gardoni and Y. Fujino. (2000). Base isolation system with shape memory alloy device for elevated highway bridges, Engineering Structures 22 , pp. 222–229.
2) Song, G., Ma, N., Li, H.N. (2006). Applications of Shape Memory Alloys in Civil Structures. *Engineering Structures*. 28,1266-1274.
3) Motahari, S. A. and Ghassemieh, M. (2007). Multilinear One-dimensional Shape Memory Material Model for Use in Structural Engineering Applications. *Engineering Structures*, 29 ,904–913.
4) Paiva, A. and Savi M.A. (2006). An Overview of Constitutive Models for Shape Memory Alloys. *Mathematical Problems in Engineering*, 2006,1-30.
5) Ye, L.P., and Ouyang, Y.F.(2000). "Dual seismic structure system and its parametric analysis." *Engineering Mechanics*,17(2),23-29.
6) Chen, Z.Y., Ge, H.B., and Usami, T. (2007). Study on Seismic Performance Upgrading for Steel Bridge Structures by Introducing Energy-Dissipation Members. JSCE J. of Struct. Eng., 53A.
7) JRA. (2002). *Design specification of highway bridges. Part V: seismic design*, Japan Road Association, Tokyo, Japan(in Japanese).
8) SAC. *Develop suites of time histories, SAC Joint Venture Steel Project Phase2: Project Task 5.4.1*. Draft Report prepared by Woodward-Clyde Federal Services, Pasadena, CA, 1997.
9) Usami, T. ed. (2006). *Guidelines for seismic and damage control design of steel bridges*, Japanese Society of Steel Construction, Tokyo, Japan (in Japanese).